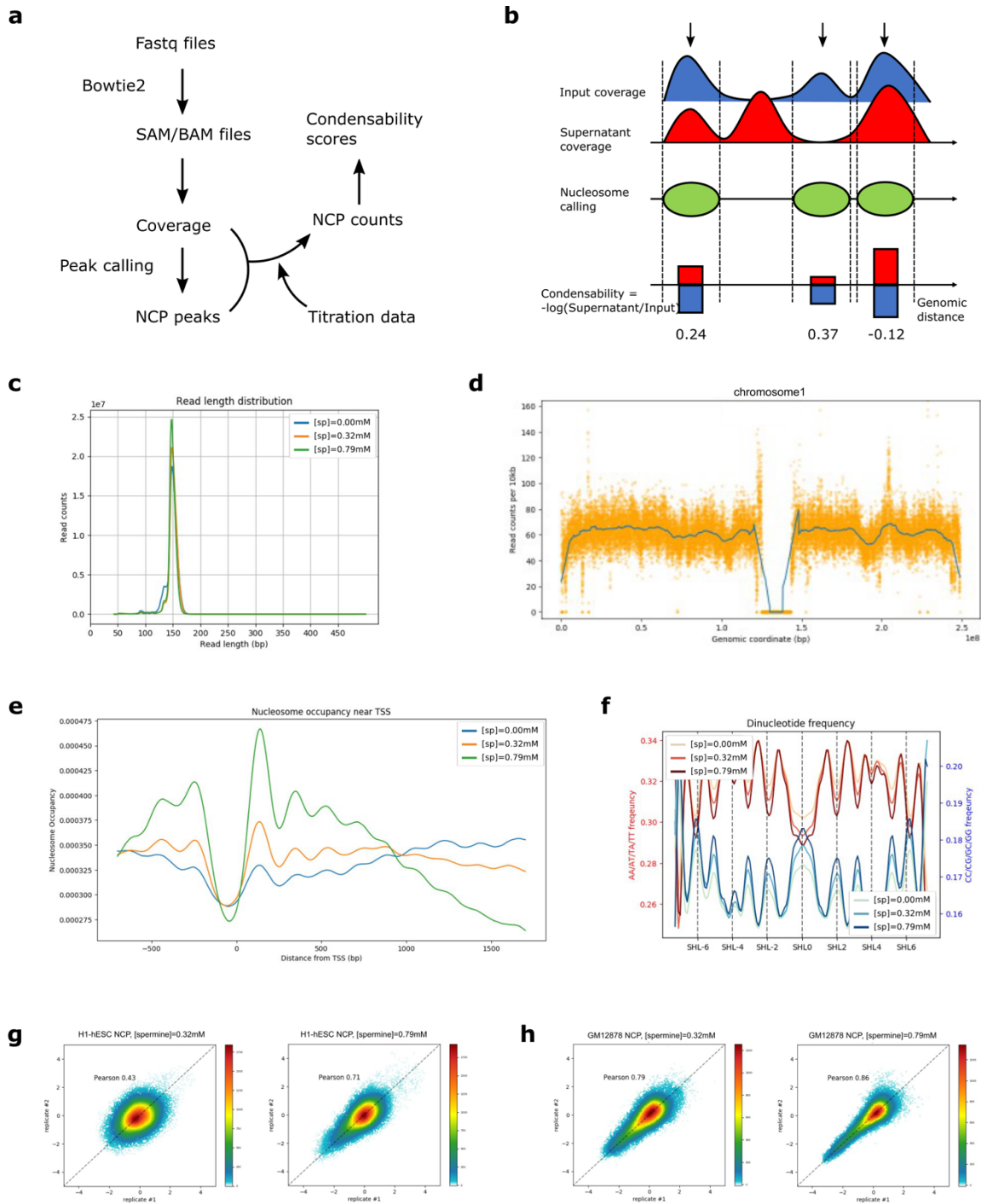


1  
2  
3  
4  
5  
6  
7  
8  
9

**Extended Data Fig. 1: Intact native mono-nucleosomes obtained by hydroxyapatite (HAP) and size-selective purification.**

**a**, After the HAP purification of MNase-treated chromatin, flow-through and elution samples were run in 2% agarose gel. **b**, Mono-nucleosomes were selected through further size-selective purification of HAP elution. Each purification step and the quality of final product was validated by running the samples in 2% agarose gel (**c**), SDS-PAGE gel showing only four histones without other proteins (**d**), and western blot for histone PTMs (**e**).



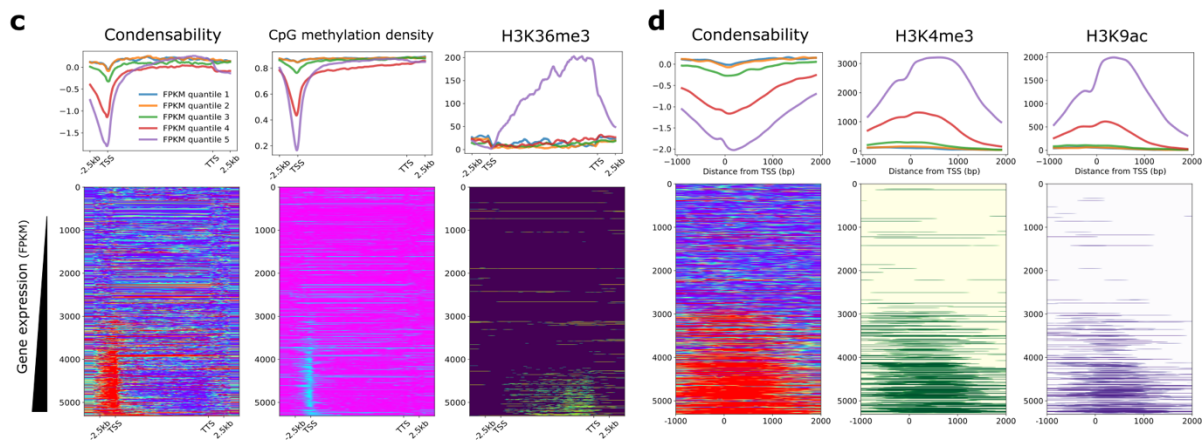
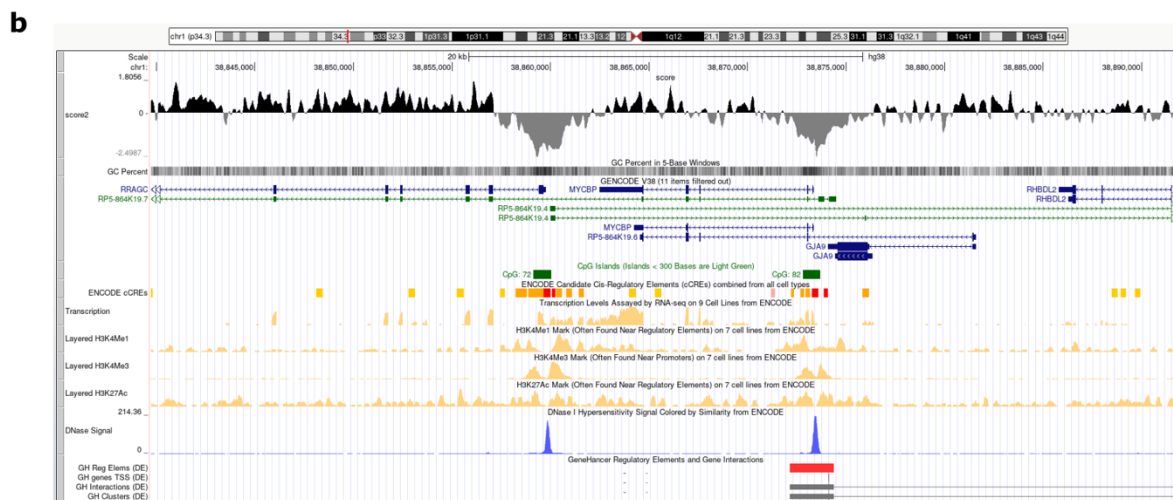
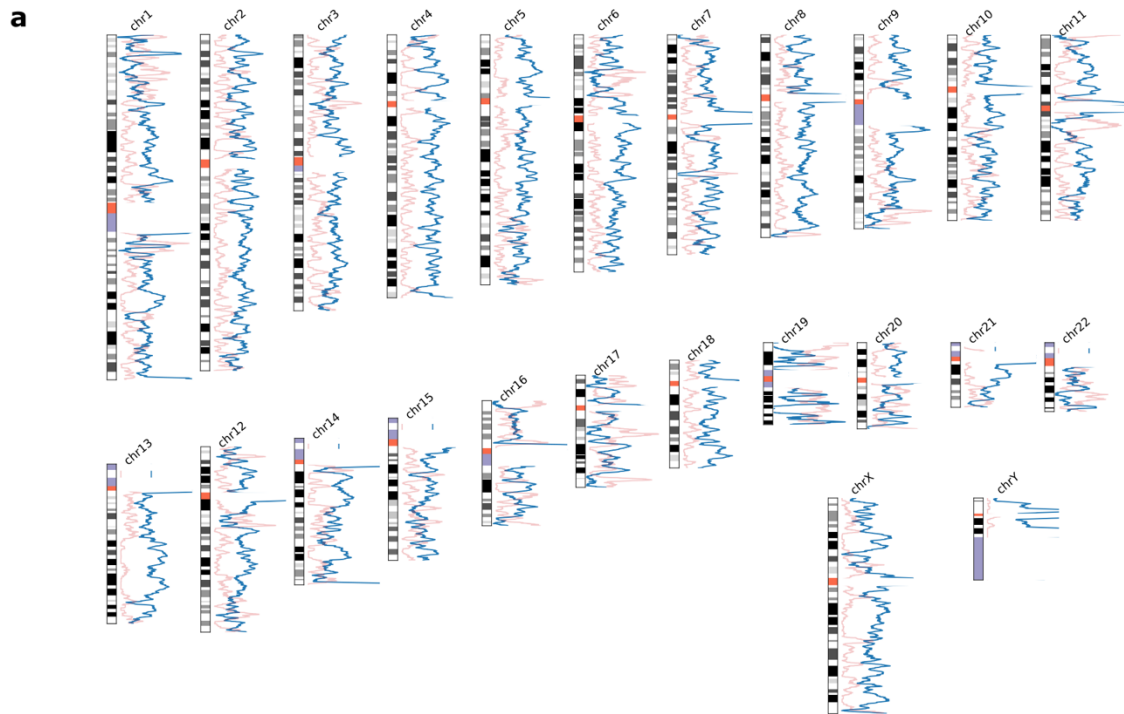
10

11 **Extended Data Fig. 2: Computational pipeline and data quality controls for condens-seq.**

12 **a,b**, The pipeline of Condense-seq analysis is composed of (i) reads alignment by Bowtie2, (ii) coverage  
 13 calculations, (iii) mono-nucleosome peak calling for each local maximum of input coverage, (iv) absolute  
 14 nucleosome count estimation using coverage area and soluble fraction changes, and (v) compute  
 15 condensability score as minus log of soluble fraction after condensation for each nucleosome. For the  
 16 quality control of mono-nucleosome samples, we checked that the length distribution of nucleosomal DNA  
 17 is mostly at 150 bp (**c**), reads are covered evenly along the genome (**d**), nucleosome positioning shows the  
 18 signature properties such as the nucleosome free region (NFR) near the transcription start site (**e**), and the

19 periodicity of AT-rich versus GC-rich dinucleotides in nucleosomal DNAs (**f**). Correlation between replicates  
20 of Condense-seq measurements on H1-hESC (**g**) and GM12878 (**h**) are shown for condensabilities  
21 determined for 0.32 mM spermine and 0.79 mM spermine.

22

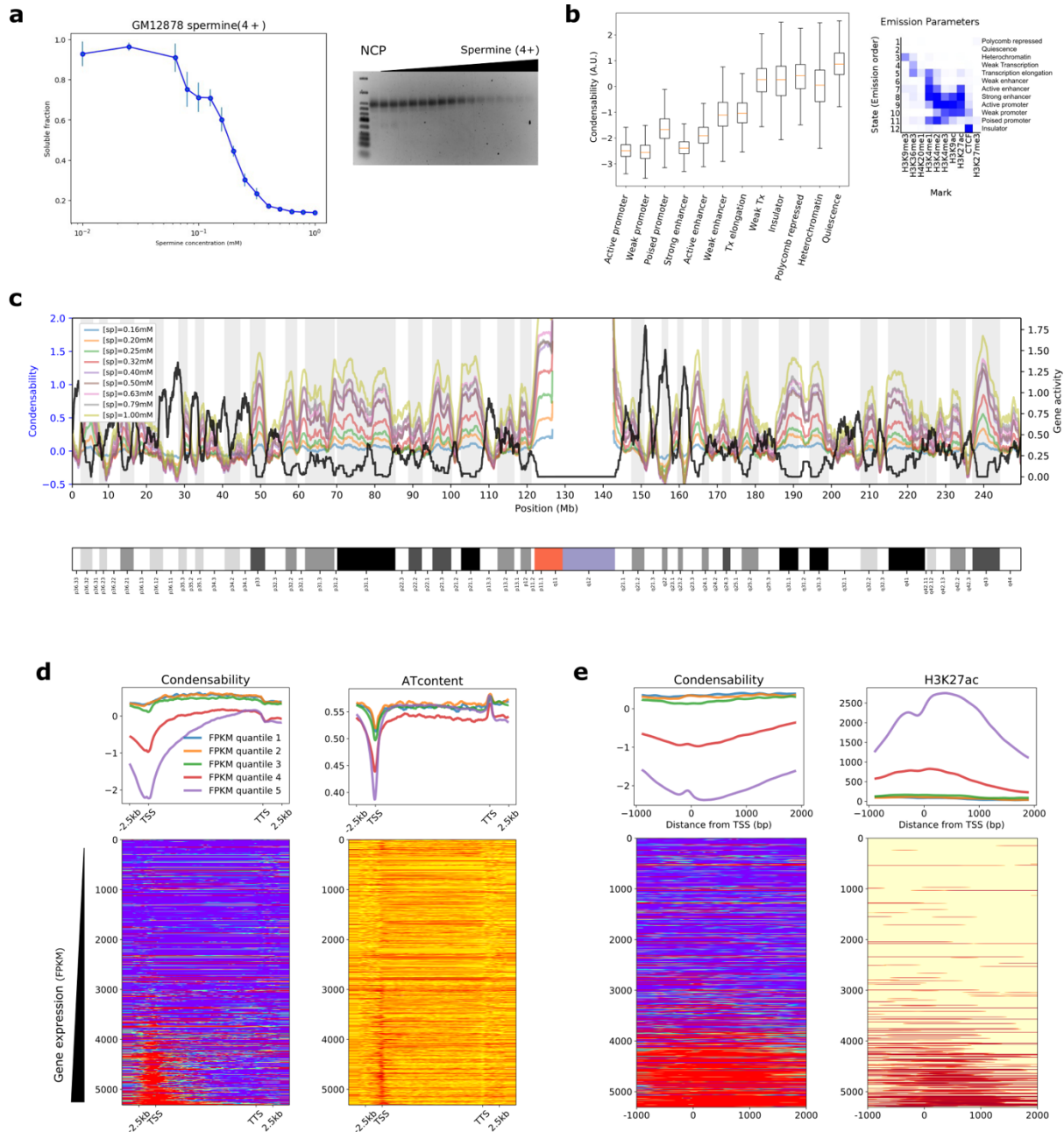




24 **Extended Data Fig. 3: Condensability scores of H1-hESC across all chromosomes and**  
25 **correlations with gene expression and other epigenetic marks near the TSS.**

26 **a**, Comparison between condensability (blue) and transcription level (red) along all chromosomes. **b**,  
27 Snapshot of UCSC genome browser for the condensability profile along with many other cis-regulatory  
28 elements. **c,d**, All genes in chromosome 1 were grouped into five quantiles according to the transcription  
29 level (quantile 1 through 5 for increasing transcription). (top) Condensability, meCpG fraction, H3K36me3,  
30 H3K4me4 and H3K9ac along the transcription unit coordinate averaged for each quantile. (bottom) Heat  
31 maps show the same quantities for each gene, rank ordered with increasing condensability. TSS  
32 (transcription start site), TTS (transcription termination site). Views zoomed around TSS are shown in **(d)** .

33

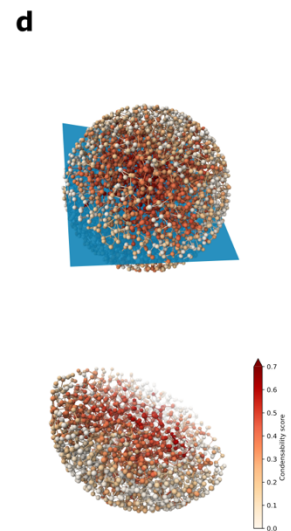
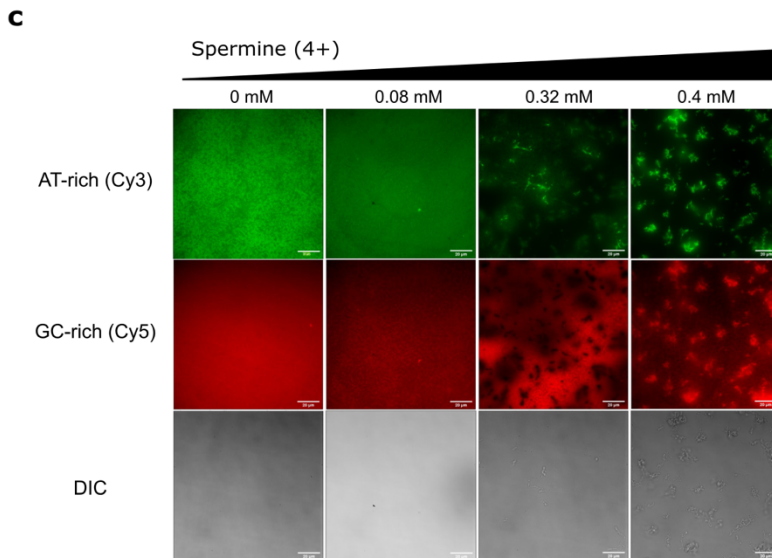
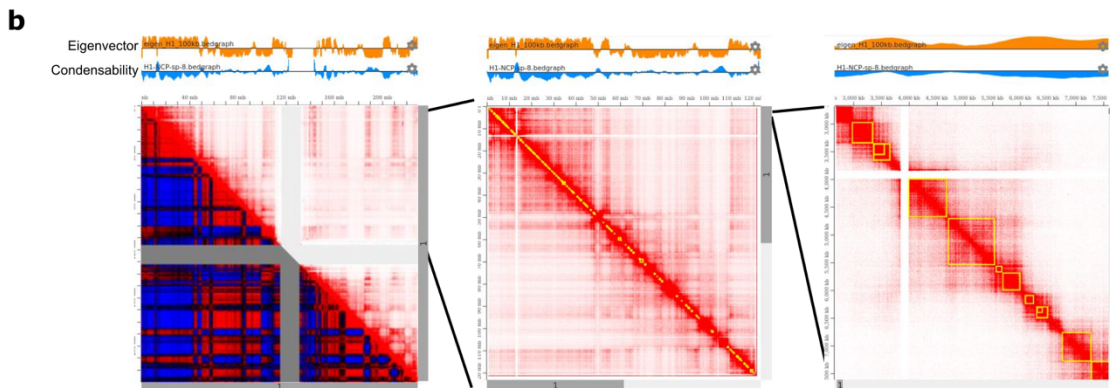
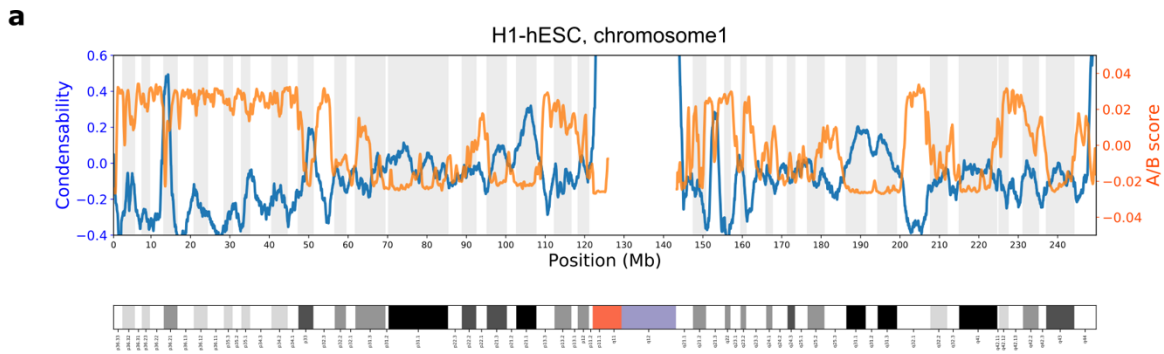


34

35 **Extended Data Fig. 4: Condense-seq measurement of native mono-nucleosomes from GM12878**  
 36 **cells and the comparison between nucleosome condensability and their chromatin states.**

37 **a**, Native mono-nucleosomes were purified from GM12878 cell line, and the condensation was induced by  
 38 adding spermine. Soluble fractions were measured using UV-VIS spectroscopy (left) and ran in the 2%  
 39 agarose gel (right). **b**, Genomic nucleosomes were grouped according to their ChromHMM chromatin states  
 40 based on the combination of various PTMs. Their condensabilities are shown in box plot for each chromatin  
 41 state. **c**, The condensability score was plotted over human chromosome1 for different spermine titration  
 42 points (colored lines) and compared with the gene expression level (black line). The condensability profiles  
 43 from TSS to TTS (**d**) near TSS (**e**) for five quantiles based on the gene expression levels in the GM12878  
 44 cell line. Also shown at AT content and H3K27ac profiles.

45



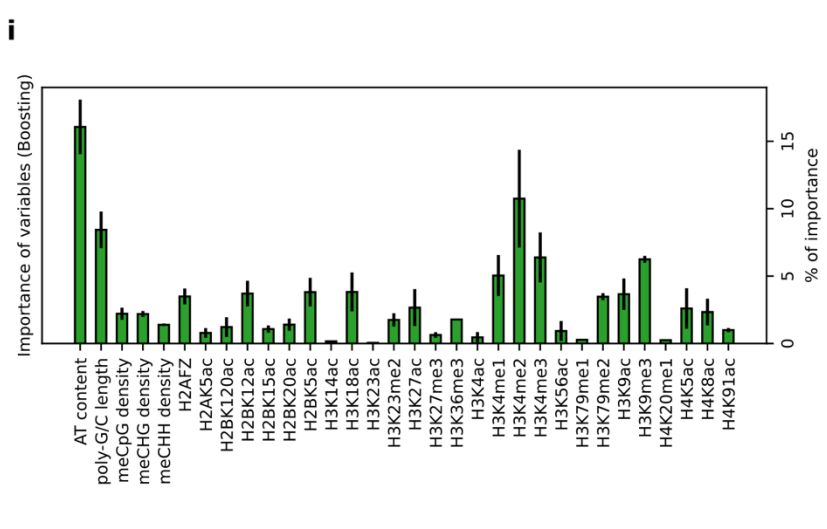
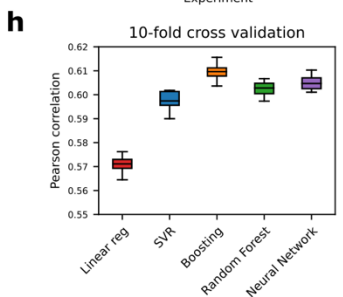
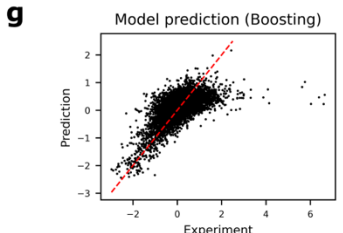
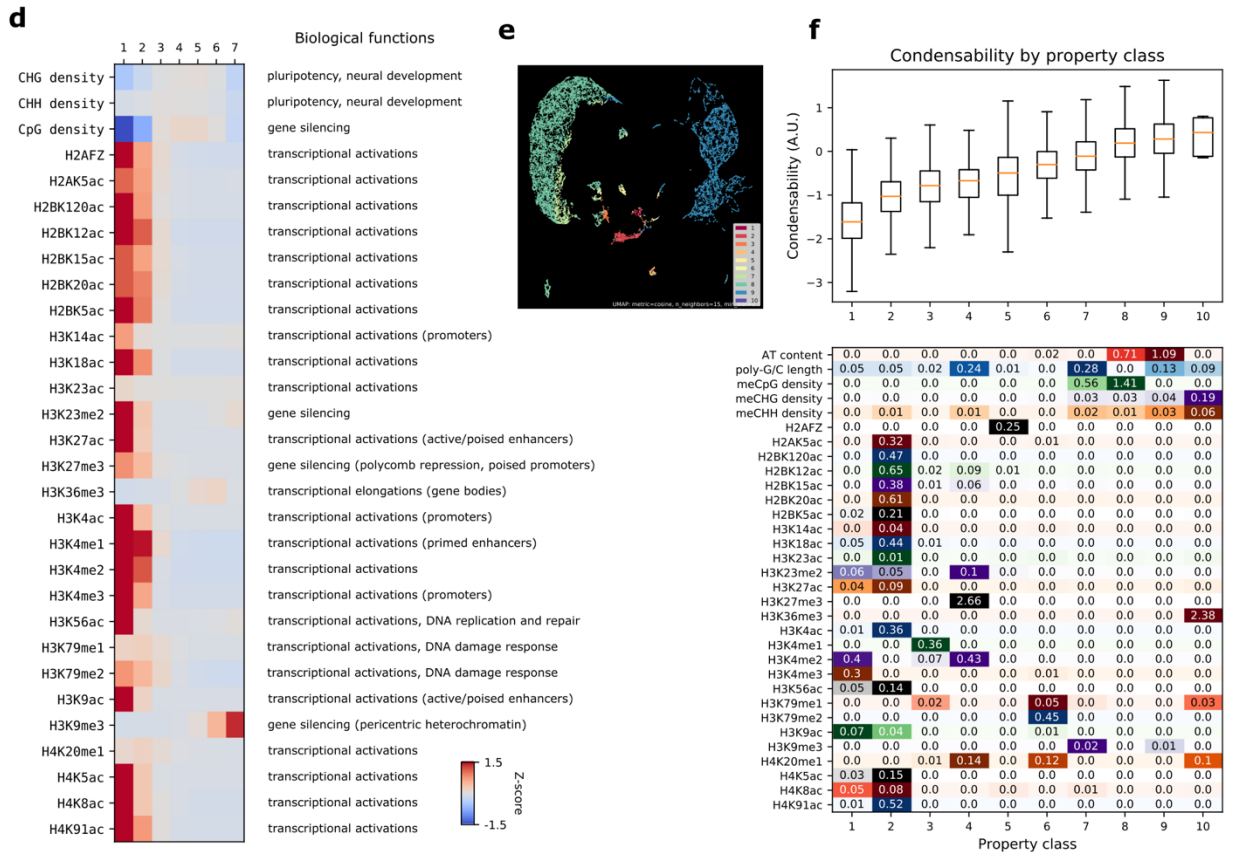
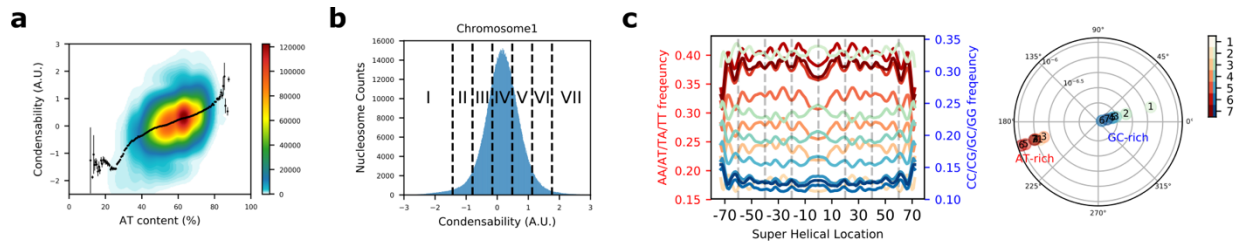
46

47 **Extended Data Fig. 5: Spatial separation of molecules promoted by condensability difference to**  
 48 **compartmentalize the genome.**

49 H1-hESC condensability (blue) and A/B compartment scores based on Micro-C data (orange) in mega  
 50 base-pair resolution of chromosome 1 (a) and finer resolution (b). **c**, PCR amplified AT-rich (Cy3 labeled)  
 51 and GC-rich (Cy5 labeled) DNAs were equally mixed and condensed in various spermine concentrations.  
 52 For each condition, DNA condensates were imaged using wide-field microscope. As spermine  
 53 concentration increased, AT-rich DNAs formed a condensed core first, and GC-rich DNAs condensed over

54 the AT-rich core at higher spermine concentrations, promoting the spatial separation between AT-rich  
55 versus GC-rich condensate. **d**, Chromosome polymer simulation with condense-seq data using spermine  
56 as only input (GM12878, chr12) shows that highly condensable chromatin is compacted into the core and  
57 the rest is excluded to generate spatially separate compartments (red = condensability score).

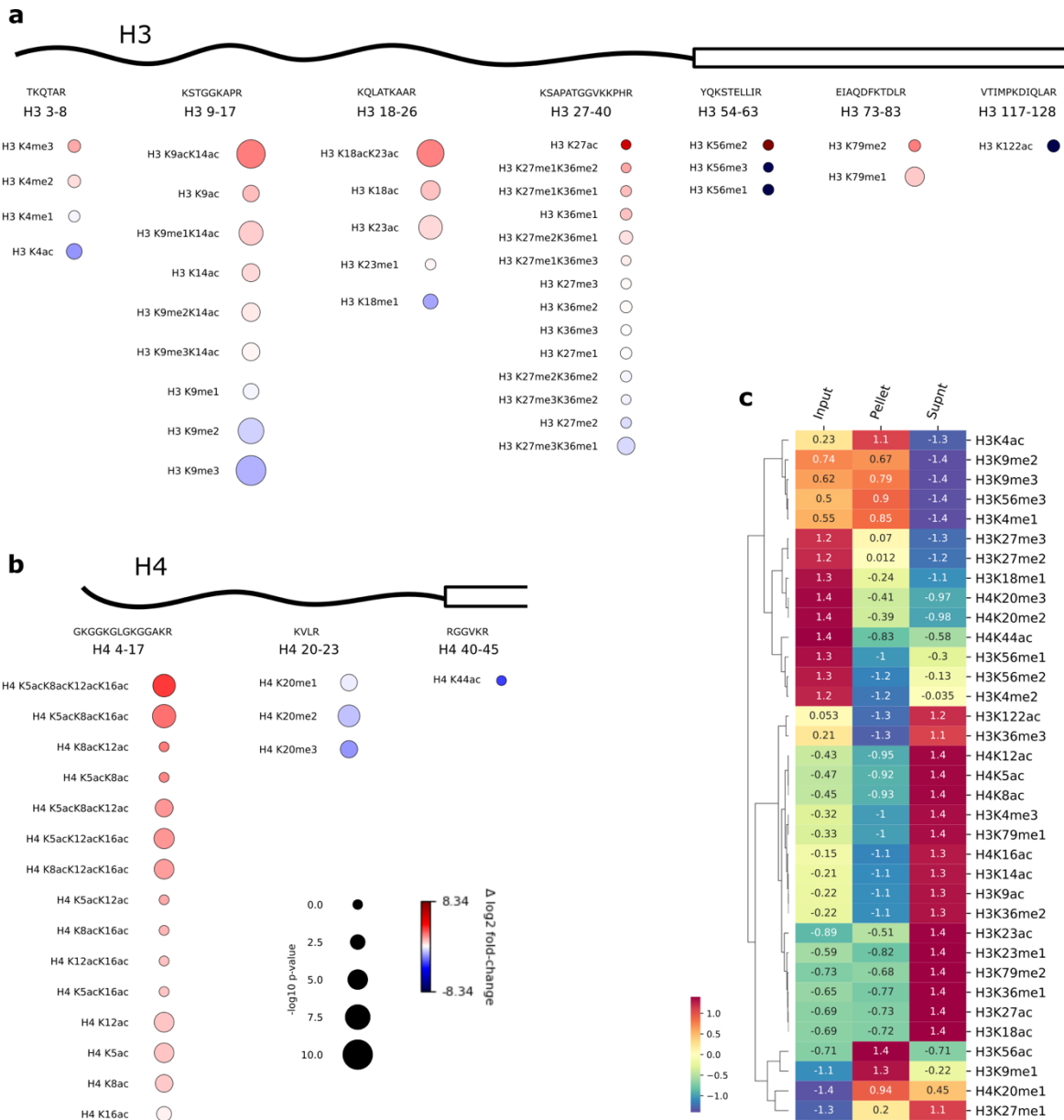
58



60 **Extended Data Fig. 6: Deciphering the genetic and epigenetic determinants of genomic**  
61 **nucleosome condensation.**

62 **a**, Scatter plot of the condensability of mono-nucleosomes in chromosome 1 and the AT contents of  
63 corresponding nucleosomal DNA. **b**, The nucleosome population was partitioned into seven partitions, from  
64 low to high condensability. The periodicity of AT-rich versus GC-rich dinucleotides was analyzed. The  
65 results for each partition (**c**, left), and its amplitude and phase were computed using Fourier transformation  
66 and represented in polar plot (**c**, right, radius: amplitude, angle: phase). **d**, The enrichment analysis of all  
67 DNA methylation and histone ChIP-seq data available in ENCODE over different condensability partitions  
68 from low to high (1-7 partitions in **b**). **e**, After randomly selecting 1% of the mono-nucleosomes in  
69 chromosome 1, their genetic and epigenetic features were projected into two-dimensional scatter plots  
70 through UMAP embedding. Each color represents one of the property classes of the NMF analysis shown  
71 in panel **f**. **f**, The genetic and epigenetic features of all mono-nucleosomes in chromosome 1 were linearly  
72 decomposed into 10 property classes by NMF algorithms. Each property class has a specific combination  
73 of features, as shown in the matrix (lower panel). All nucleosomes were clustered into each representative  
74 property class with the biggest contributions. After clustering, nucleosome condensabilities were plotted as  
75 boxplot for each class (upper panel). **g–i**, Multivariate linear regression (linear reg), Supported Vector  
76 Machine regression (SVM), gradient boosting regression (Boosting), random forest regression (Random  
77 Forest), and neural networks were used to predict nucleosome condensability. All showed similar  
78 correlations between experimental values and predictions in a 10-fold cross-validation (**g,h**). The  
79 importance of genetic–epigenetic features in prediction was computed using the boosting method (**i**).

80



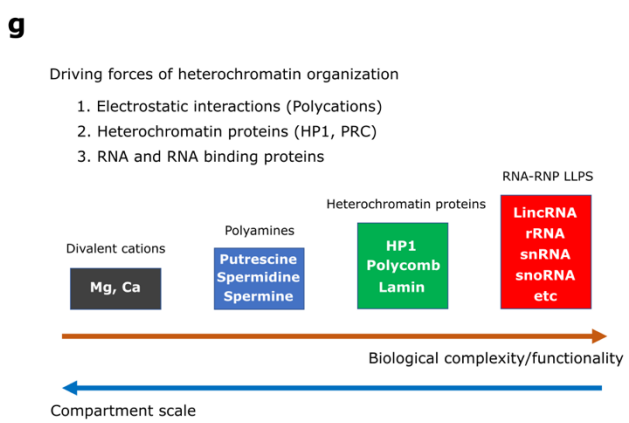
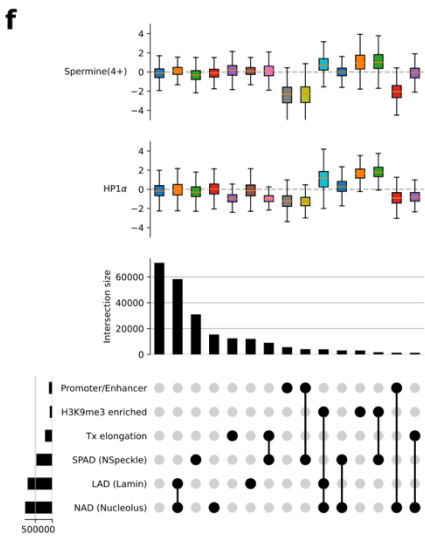
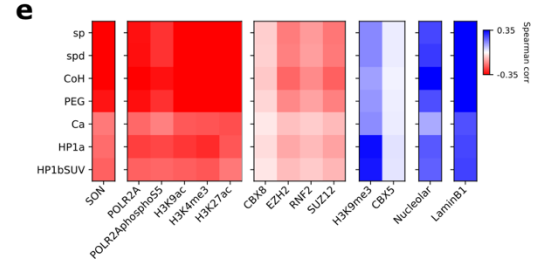
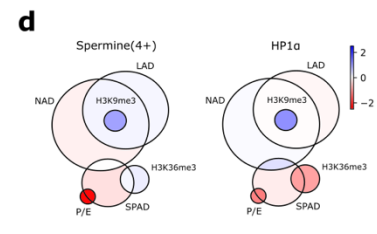
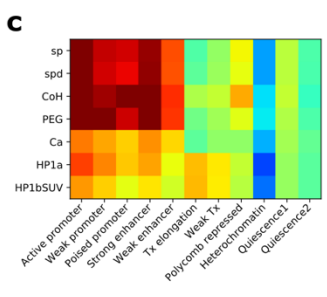
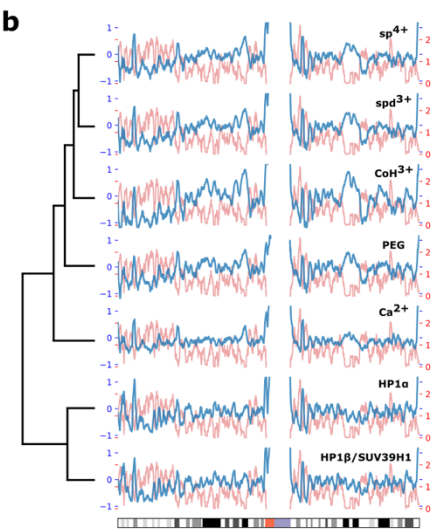
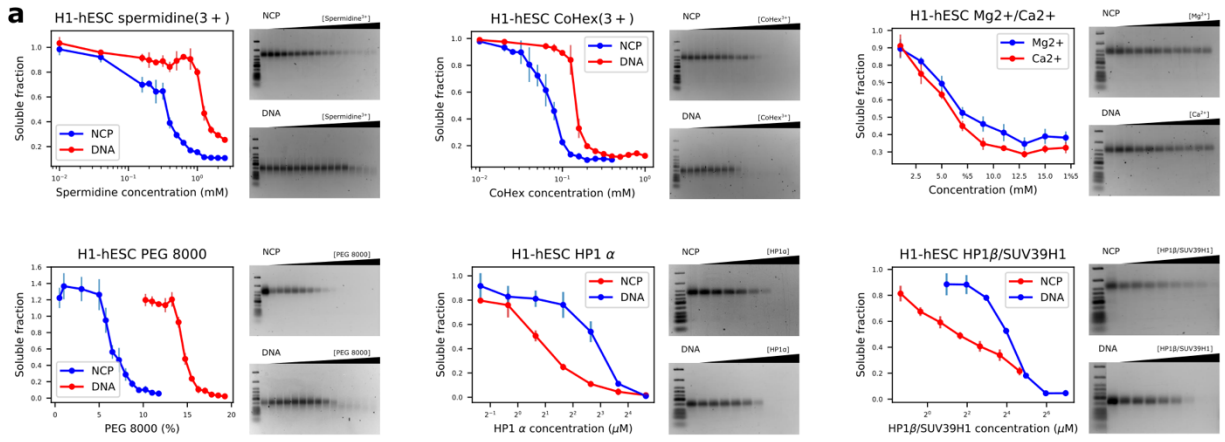
81

82 **Extended Data Fig. 7: Mass spectrometry identification of histone PTM marks with biased**  
 83 **enrichment during native mononucleosome condensation experiments.**

84 **a,b**, Histone PTM marks detected in each histone H3/H4 peptides are shown. Its relative enrichment  
 85 difference compared with the unmodified peptide is represented by color (red: more enriched in  
 86 supernatant, blue: more depleted in supernatant) and its signification is represented by the size of bubble  
 87 ( $-\log$  p-value). **c**, Combinatorial histone PTM enrichment data was aggregated into single PTM  
 88 modifications, and the relative enrichment in each phase of condensation (input/pellet/supernatant) is  
 89 shown in the z-score heat map.

90





91

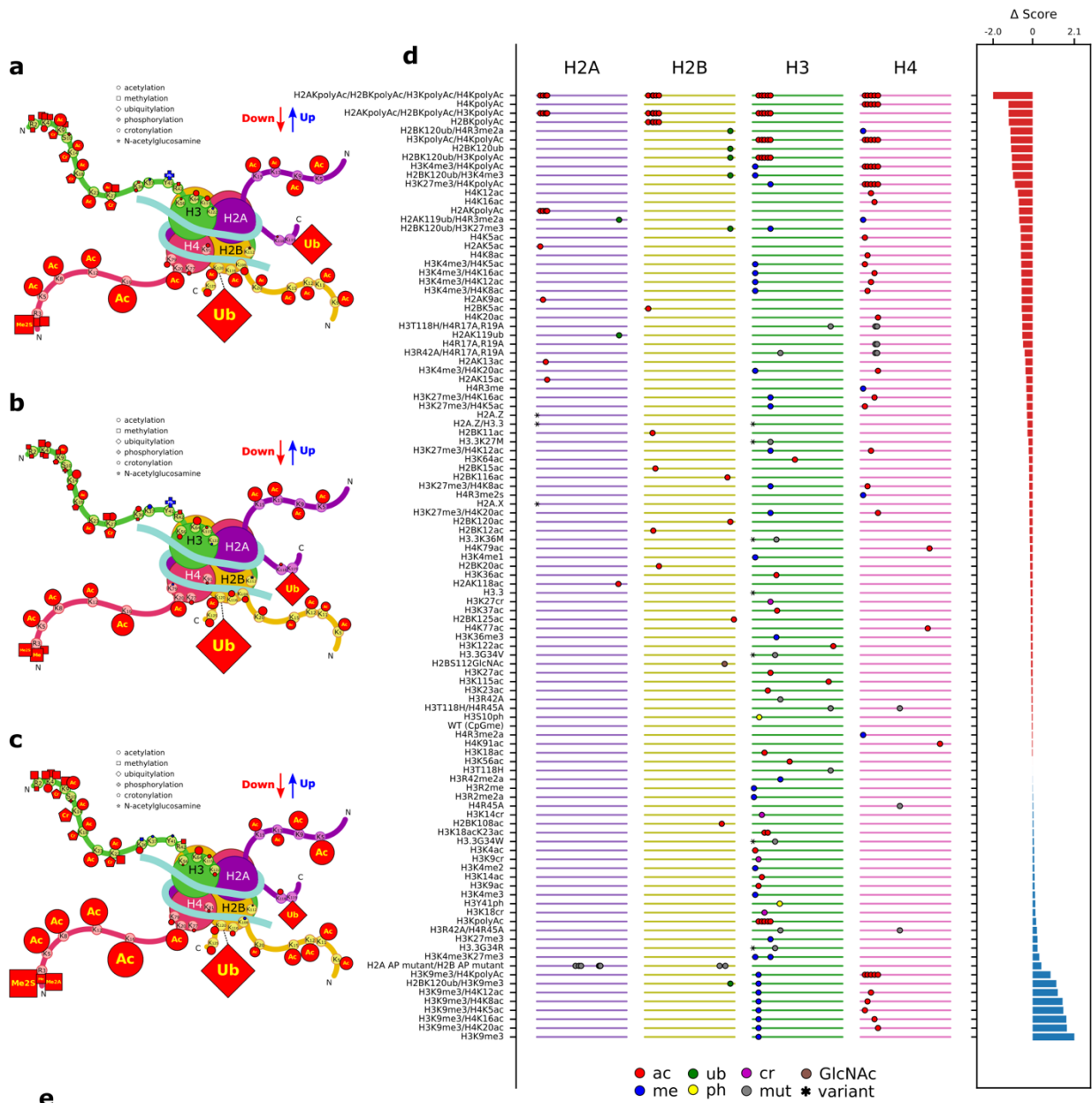
92

93

**Extended Data Fig. 8: Condense-seq of H1-hESC native mono-nucleosomes using various condensing agents.**

94 **a**, The soluble fraction of nucleosomes was measured by titrating the various condensing agents other than  
95 spermine, including spermidine, cobalt-hexamine, magnesium/calcium, PEG 8000, and HP1 $\alpha$ , HP1 $\beta$  with  
96 SUV39H1 complex. **b**, Condensability scores were computed in 10kb resolution and plotted over  
97 chromosome 1 (blue) and compared with the gene expression level (red). Hierarchical clustering of the  
98 condensability profile shows that all ionic condensing agents (spermine/spermidine/cobalt-  
99 hexamine/PEG/calcium) are clustered together but other protein-based condensing agents (HP1 $\alpha$  and  
100 HP1 $\beta$ ) are clustered in a separate group. Comparison of condensability scores across various chromatin  
101 states (**c**) and various nuclear compartments (**d**, LAD: lamin-associated domain, NAD: nucleolar-associated  
102 domain, SPAD: nuclear speckle-associated domain, P/E: promoter or enhancer) for different condensing  
103 agents. **e**, Correlations between nucleosome condensability and the enrichment of other nuclear  
104 compartment hall mark proteins are represented as heat map. **f**, Upset plot of intersections between various  
105 nuclear compartments and the corresponding nucleosome condensabilities by spermine and HP1 $\alpha$  shown  
106 as bar plots. **g**, Hypothetical hierarchal model of the biophysical driving force of chromatin organization: At  
107 a large scale, chromatin is compartmentalized via ubiquitous charge–charge interactions, but other proteins  
108 and RNAs are involved to generate sub-compartments that are smaller in scale but more specific function  
109 directed.

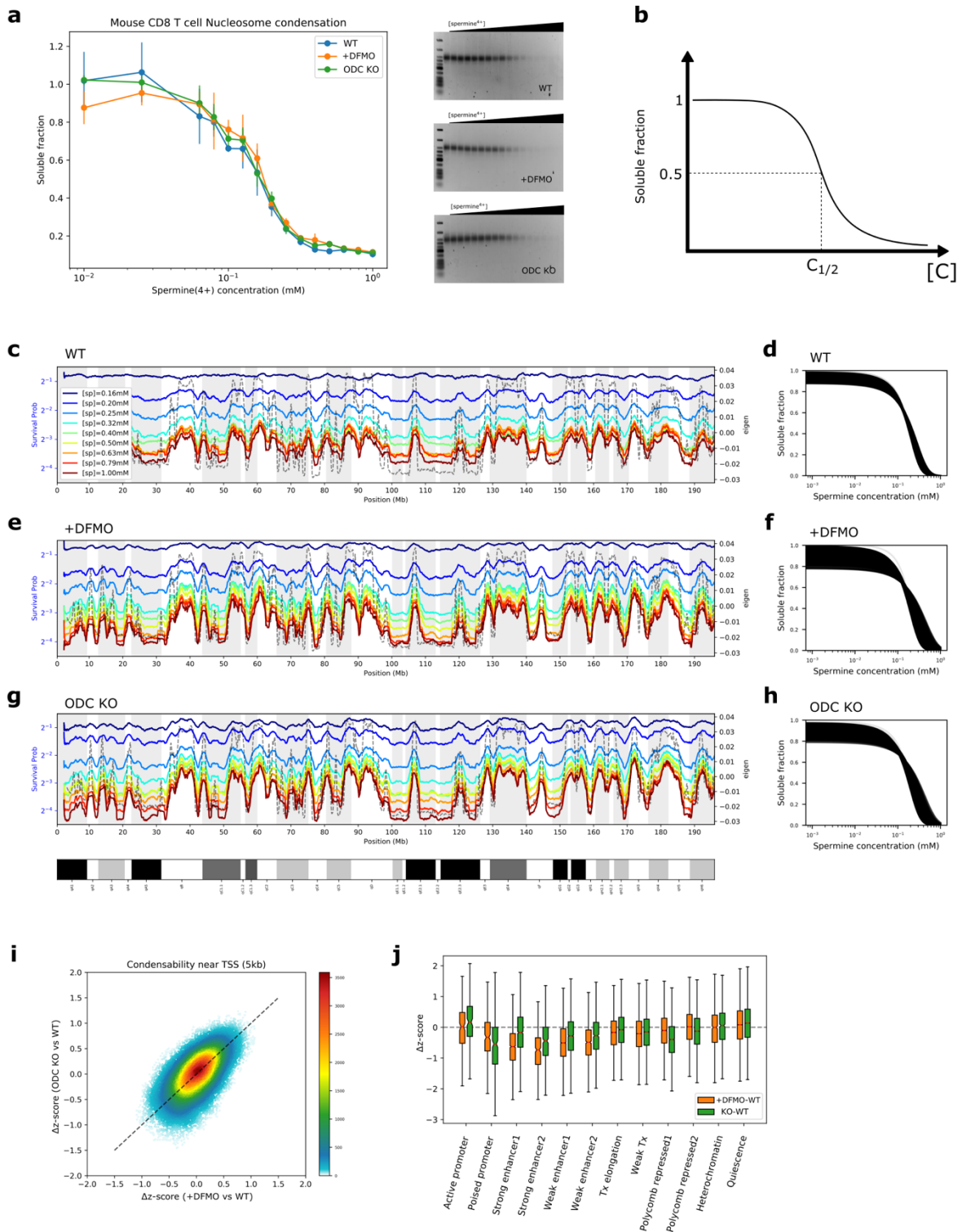
110



112 **Extended Data Fig. 9: Summary of histone PTM effects on the nucleosome condensation by**  
113 **various condensing agents on the synthetic nucleosome library with PTM marks.**

114 The effects of single PTMs on nucleosome condensation are depicted by the cartoons (**a**: spermidine, **b**:  
115 cobalt-hexamine, **c**: PEG 8000 as the condensing agent). Each symbol represents different types of PTMs  
116 as shown in the legend, and the size is proportional to the strength of effects. The colors of the marks  
117 indicate the direction of the effect (red: decreases condensation, blue: increases condensation) compared  
118 with the unmodified control. **d**, All condensability scores of the PTM library using HP1 $\alpha$  as a condensing  
119 agent are summarized in the ladder bar plot. The library members are sorted from the lowest to the highest  
120 condensability scores from top to bottom. On the left panel, the ladder-like lines represent each histone  
121 subunit peptide from N-terminal (left) to the C-terminal (right). Each mark on the line indicates the location  
122 of the PTMs and the shape of the marks represents the PTM type (ac: acetylation, me: methylation, cr:  
123 crotonylation, ub: ubiquitylation, ph: phosphorylation, GlcNAc: GlcNAcylation, mut: amino acid mutation,  
124 var: histone variant). On the right panel, differences in the condensability score compared with the  
125 unmodified control are shown as bar plots for each member of the library. **e**, PCA analysis was conducted  
126 by combining the condensability scores of all five condensing agents (spermine/spermidine/cobalt-  
127 hexamine/PEG 8000/HP1 $\alpha$ ) into the five-dimensional state vector. In the PCA plot, each member of the  
128 library is represented by a symbols according to categories such as canonical wild-type nucleosome (WT),  
129 wild type with CpG methylation (WT+CpGme), mutations on wild type (WT+mut), nucleosome with histone  
130 variants (Var), mutations on histone variants (Var+mut), Acidic patch mutants (AP mutants), and  
131 nucleosomes with acetylation on H2A/B dimer (H2A/Bac), acetylation on H3 (H3ac), acetylation on (H4ac),  
132 having poly-acetylation (KpolyAC), methylation on H3 (H3me), methylation on H4 (H4me), acetylation on  
133 H4 and methylation on H3 (H4ac + H3me), crotonylation on H3 (H3cr), GlcNAcylation (GlcNAc),  
134 phosphorylation on H3 (H3ph), and ubiquitylation (+ub), all of which are shown in the figure legend. **f**,  
135 Comparison of condensability scores across different condensing agents. Scatter plots of condensability  
136 across different condensing agents are shown in the lower triangle, and the corresponding Spearman's  
137 correlations are shown in the upper triangle of the matrix.

138



139

140 **Extended Data Fig. 10: Condense-seq measurements of nucleosomes purified from mouse CD8<sup>+</sup> T**  
 141 **cells.**

142 **a**, Soluble fractions were measured via UV-VIS spectroscopy and run in 2% agarose gel after condensation  
 143 in various spermine concentrations. **b**, Condensation point ( $C_{1/2}$ ) is defined by the concentration of  
 144 condensing agent when the soluble fraction is half the input, so it is reversely correlated with condensability

145 score. **c–h**, Soluble fractions of nucleosomes in various spermine concentrations were calculated and  
146 plotted over chromosome 1 in 10kb resolution.  $C_{1/2}$  was computed for each bin after fitting the soluble  
147 fraction change with a logistic function as shown fitting curves of all bins (**d, f, h**), and polyamine deficient  
148 conditions show broader distribution of condensation points. (**c, d**: wild type control, **e, f**: +DFMO, **g, h**:  
149 ODC KO) **i**, The scatter plot of  $\Delta$  z-score of condensability near TSS shows a high correlation between  
150 +DFMO and ODC KO. **j**, The  $\Delta$  z-score of condensabilities is computed as the difference between the  
151 standardized condensability of +DFMO or ODC KO conditions and the wild type control and then  
152 categorized into the corresponding ChromHMM chromatin states.